CIMPA

Epi-SCIENCE
THE SCIENCE BEHIND POPULATION HEALTH

revistas.ucr.ac.cr/index.php/repiscience

The Impact of Short-Term Mobility and Healthcare Access on Epidemic Containment

Arjun Garg[1], Baltazar Espinoza[2]

[1]*Thomas Jefferson High School for Science and Technology*
[2]*Biocomplexity Institute, University of Virginia*

be8dq@virginia.edu

Submitted: 06/02/2025; Accepted: 05/28/2026
DOI: https://doi.org/10.15517/18cgna44

Abstract

The recent pandemics remind us that the speed and extent of infectious disease spread heavily depend on human mobility patterns. Despite their long history, mobility restrictions have not always been successful in controlling disease spread. Understanding the implications of mobility restrictions on the geographic distribution of secondary infections, in relation to healthcare availability and quality, is critical for effective disease management.

In this study, we explore the impact of short-term travel between two economically distinct communities on the transmission and containment of epidemics. We implemented a two-community mathematical model, where socio-economic conditions influence transmission rates and healthcare access. The model tracks individuals' place of residency by incorporating the proportion of time each resident spends traveling.

We found that, in scenarios that amplify populations' disparities, the final epidemic size shows non-monotonic behavior with respect to mobility. Differences in population sizes amplify these effects, the larger population dominates disease dynamics, making mobility restrictions less effective in certain scenarios.

Moreover, travel times that reduce the final epidemic size (relative to the isolation scenario) depend on the population's relative sizes and infection rates. Moreover, we found that treatment interventions mitigate infection peaks across both groups but fail to fully overcome disparities.

Our results suggest that investing in treatment access for low-income communities is more effective in reducing the total final epidemic size than equivalent investments in high-income communities, especially when low-income populations are larger.

Keywords: Epidemic modeling; Mobility restrictions; Healthcare disparities; Reproduction number; Socioeconomic heterogeneity.

CIMPA

Epi-SCIENCE
THE SCIENCE BEHIND POPULATION HEALTH

revistas.ucr.ac.cr/index.php/repiscience

El impacto de la movilidad a corto plazo y el acceso a la atención médica en el control de epidemias

Arjun Garg[1], Baltazar Espinoza[2]

[1]*Thomas Jefferson High School for Science and Technology*
[2]*Biocomplexity Institute, University of Virginia*

be8dq@virginia.edu

Enviado: 02/06/2025; Aceptado: 28/05/2026
DOI: https://doi.org/10.15517/18cgna44

Resumen

Las recientes pandemias nos recuerdan que la velocidad y el alcance de la propagación de enfermedades infecciosas dependen en gran medida de los patrones de movilidad humana. A pesar de su larga historia, las restricciones a la movilidad no siempre han logrado controlar la propagación de enfermedades. Comprender las implicaciones de estas restricciones en la distribución geográfica de las infecciones secundarias, en relación con la disponibilidad y la calidad de la atención médica, es fundamental para una gestión eficaz de las enfermedades.

En este estudio, exploramos el impacto de los viajes de corta duración entre dos comunidades con características económicas distintas en la transmisión y contención de epidemias. Implementamos un modelo matemático de dos comunidades, donde las condiciones socioeconómicas influyen en las tasas de transmisión y el acceso a la atención médica. El modelo registra el lugar de residencia de los individuos incorporando la proporción de tiempo que cada residente dedica a viajar.

Descubrimos que, en escenarios que amplifican las disparidades entre poblaciones, el tamaño final de la epidemia muestra un comportamiento no monótono con respecto a la movilidad. Las diferencias en el tamaño de las poblaciones amplifican estos efectos: la población más grande domina la dinámica de la enfermedad, lo que hace que las restricciones a la movilidad sean menos efectivas en ciertos escenarios.

Además, los tiempos de viaje que reducen el tamaño final de la epidemia (en comparación con el escenario de aislamiento) dependen del tamaño relativo de las poblaciones y de las tasas de infección. Además, observamos que las intervenciones de tratamiento mitigan los picos de infección en ambos grupos, pero no logran superar por completo las disparidades.

Nuestros resultados sugieren que invertir en el acceso al tratamiento para las comunidades de bajos ingresos es más eficaz para reducir el tamaño total de la epidemia que inversiones equivalentes en comunidades de altos ingresos, especialmente cuando las poblaciones de bajos ingresos son más numerosas.

Palabras clave: Modelado epidémico; Restricciones de movilidad; Disparidades en atención médica; Número de reproducción; Heterogeneidad socioeconómica.

1. Introduction

Infectious disease outbreaks, from the 1918 influenza pandemic, the 2003 SARS epidemic, and the recent COVID-19 pandemic, have heightened the pivotal role of human mobility in shaping epidemic dynamics [1, 2, 3]. Short-term mobility, characterized by daily or weekly travel between communities, is particularly critical in scenarios where populations with differing socioeconomic conditions interact closely. For instance, urban slums adjacent to affluent neighborhoods, such as the Dharavi slum in Mumbai, India, or the townships bordering Cape Town, South Africa, exemplify settings where short-term mobility drives disease transmission across economic divides [4]. Similarly, in the United States, migrant workers traveling between rural agricultural communities and urban centers, or commuters moving between boroughs like the Bronx and Manhattan in New York City, create pathways for disease spread that are amplified by disparities in healthcare access [5]. These scenarios highlight the need to understand how mobility restrictions, often implemented as a first line of defense, interact with socioeconomic factors to influence epidemic outcomes [6, 7].

Mobility restrictions have a long history as a public health strategy, yet their effectiveness remains inconsistent [1]. While measures like travel bans and lockdowns can reduce transmission in the short term, they often fail to account for the complex interplay of socioeconomic disparities, population sizes, and healthcare access [2, 8]. For example, low-income communities may prioritize immediate economic survival over compliance with mobility restrictions, leading to sustained disease transmission [9]. Moreover, the quality and availability of healthcare significantly influence disease outcomes, with high-income groups often benefiting from better access to testing, treatment, and preventive measures [10, 11]. These disparities are further compounded by biological factors, such as variations in the gut microbiome, which can affect disease susceptibility and treatment efficacy. Studies have shown that lower socioeconomic status (SES) is associated with distinct microbiome profiles, potentially increasing vulnerability to infectious diseases like COVID-19 [12, 13].

The interplay between mobility and healthcare access is particularly pronounced in heterogeneous populations. In regions governed by a single health authority, such as the metropolitan areas of São Paulo, Brazil, or Johannesburg, South Africa, stark differences in living conditions coexist within close proximity [4]. Here, short-term mobility—such as daily commutes or informal trade—can exacerbate disease spread, particularly when low-income communities face higher transmission risks due to crowded living conditions or limited sanitation. Internationally, mobility restrictions are often designed to protect specific jurisdictions rather than minimize global epidemic

size, as seen in country-specific travel bans during the early stages of COVID-19 [7, 14]. Such measures may reduce local disease burden but can inadvertently increase overall transmission by disrupting resource sharing or coordinated responses [1].

This study aims to shed light on these challenges by modeling the impact of short-term mobility between two economically distinct communities on epidemic transmission and containment. Using a two-community mathematical model, we incorporate socioeconomic disparities through differences in transmission rates, population sizes, and healthcare access. The model tracks individuals' daily proportion of time traveling and captures the proportion of time spent in each community, serving as a proxy for exposure to community-specific risks [1, 6, 15, 16]. By analyzing the basic reproduction number ($\mathcal{R}_0$) and the total final epidemic size, we aim to identify mobility and treatment strategies that minimize disease burden while addressing health inequities. Our findings have implications for public health policy, offering insights into how targeted investments and tailored mobility interventions can balance epidemic control with socioeconomic considerations, particularly in settings where short-term mobility is a dominant driver of disease spread [8].

2. Methods

2.1. Two-community epidemic model

The disease course assumes susceptible individuals (S) become infected (I_i) at community-specific rates β_i, may receive treatment at rate α_i to enter the treated compartment (T_i), and recover (R_i) from (I_i) at rate γ_i or from (T_i) at rate $\kappa_i > \gamma_i$. In this study we focus on single outbreak dynamics, consequently no demographic processes are assumed. We formulated a two-community mathematical model to analyze disease dynamics across economically heterogeneous populations, incorporating treatment effects. The model is SITR for the full version with treatment and SIR as a special case without treatment ($\alpha_H = \alpha_L = 0$). Using a Lagrangian approach, we track mobility via a residency time matrix, capturing the average proportion of daily time individuals spend in each community (t_H for high-income, t_L for low-income). This proportion serves as a proxy for exposure to community-specific disease risks. t_H and t_L are the proportions of time that high-income and low-income individuals spend traveling to the other community, respectively. The model divides the population into high-income (H) and low-income (L) communities. Both of the populations are split into susceptible (S), infected (I), under treatment (T), and recovered (R) compartments, depending on their health states. Additionally, N_H and N_L represent the total population sizes of the high-income and low-income communities, respectively. The flow diagram in Figure 1 illustrates

the population health states and transitions, and these are mathematically formalized in Eqn. (1).

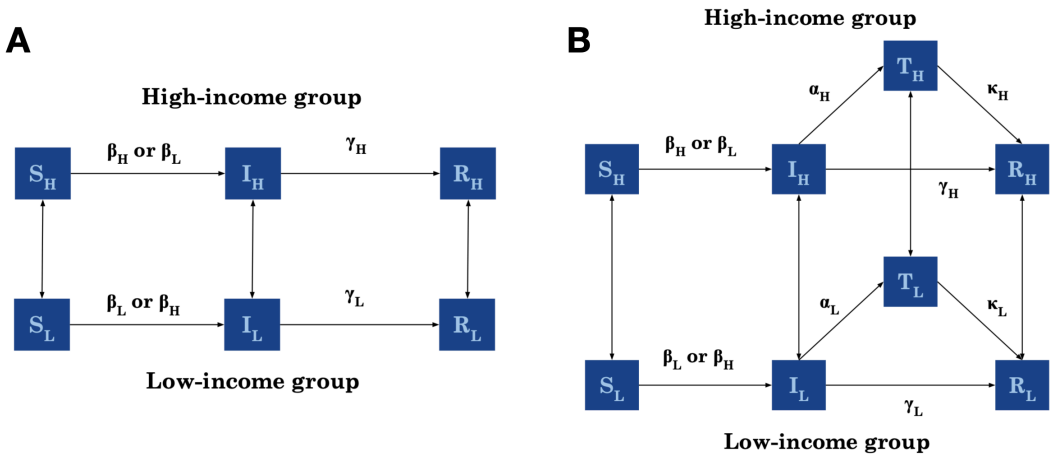

Figure 1: Two-community flow diagrams. (A) No-treatment SIR model (susceptible S, infected I, recovered R). (B) Treatment SITR model (susceptible S, infected I, treated T, recovered R). Individuals maintain their economic status during the epidemic but travel temporarily between communities, which produces cross-community infections and ultimately influence disease spread.

$$
\begin{aligned}
\dot{S_H} &= -(1-t_H)\beta_H S_H \frac{(1-t_H)I_H + t_L I_L}{(1-t_H)N_H + t_L N_L} - t_H \beta_L S_H \frac{t_H I_H + (1-t_L)I_L}{t_H N_H + (1-t_L)N_L} \\
\dot{I_H} &= (1-t_H)\beta_H S_H \frac{(1-t_H)I_H + t_L I_L}{(1-t_H)N_H + t_L N_L} + t_H \beta_L S_H \frac{t_H I_H + (1-t_L)I_L}{t_H N_H + (1-t_L)N_L} - (\gamma_H + \alpha_H) I_H \\
\dot{T_H} &= \alpha_H I_H - \kappa_H T_H \\
\dot{R_H} &= \gamma_H I_H + \kappa_H T_H \\
\dot{S_L} &= -(1-t_L)\beta_L S_L \frac{(1-t_L)I_L + t_H I_H}{(1-t_L)N_L + t_H N_H} - t_L \beta_H S_L \frac{t_L I_L + (1-t_H)I_H}{t_L N_L + (1-t_H)N_H} \\
\dot{I_L} &= (1-t_L)\beta_L S_L \frac{(1-t_L)I_L + t_H I_H}{(1-t_L)N_L + t_H N_H} + t_L \beta_H S_L \frac{t_L I_L + (1-t_H)I_H}{t_L N_L + (1-t_H)N_H} - (\gamma_L + \alpha_L) I_L \\
\dot{T_L} &= \alpha_L I_L - \kappa_L T_L \\
\dot{R_L} &= \gamma_L I_L + \kappa_L T_L
\end{aligned}
\tag{1}
$$

In this model, β_H, β_L stand for the transmission rates in high-income and low-income communities respectively, representing infection risk per contact ($\beta_L = 3\beta_H$ in baseline); γ_H, γ_L represent the natural recovery rates of infected individuals, which are assumed the same for high- and low-income populations ($\gamma_H = \gamma_L = 1/7$); t_H, t_L represent the proportion of daily time high- and low-income individuals spend traveling to the other community respectively, ($1 - t_H$, $1 - t_L$ for time in the home community); α_H, α_L stand for the high- and low-income treatment rates respectively, these are the rates at which infected individuals enter treatment; κ_H, κ_L represent the high- and low-income recovery rates under treatment ($\kappa_H = \kappa_L = 0.3$). We model healthcare access through treatment rates $\alpha_H > \alpha_L$, where high-income individuals have higher probability of entering the treated compartment.

The infection terms incorporate the full effective contact rates. For example, the rate of new infections in the high-income community is $(1 - t_H)\beta_H S_H \frac{(1-t_H)I_H + t_L I_L}{(1-t_H)N_H + t_L N_L} + t_H \beta_L S_H \frac{t_H I_H + (1-t_L) I_L}{t_H N_H + (1-t_L) N_L}$. This models infections at home and away, with denominators representing the effective population in each location during the time spent there. Treatment terms ($\alpha_H I_H, \alpha_L I_L$) represent transitions to the treated state, and recovery terms ($\kappa_H T_H, \kappa_L T_L$) model recovery from treatment. Natural recovery ($\gamma_H I_H, \gamma_L I_L$) accounts for spontaneous recovery.

2.2. Model Analysis

We computed the model's basic reproductive number $\mathcal{R}_0$ using the next-generation matrix method [17, 18, 19]. For the uncoupled communities, $\mathcal{R}_0^H = \beta_H/(\gamma_H + \alpha_H)$ and $\mathcal{R}_0^L = \beta_L/(\gamma_L + \alpha_L)$. For the combined system, $\mathcal{R}_0$ is the spectral radius of the matrix FV^{-1}, where F is the transmission matrix derived from the infection terms at the disease-free equilibrium (DFE, $S = N$, $I = T = 0$):

$$F = \begin{pmatrix} (1 - t_H)\beta_H N_H \dfrac{(1 - t_H)}{(1 - t_H)N_H + t_L N_L} & (1 - t_H)\beta_H N_H \dfrac{t_L}{(1 - t_H)N_H + t_L N_L} \\ + t_H \beta_L N_H \dfrac{t_H}{t_H N_H + (1 - t_L)N_L} & + t_H \beta_L N_H \dfrac{1 - t_L}{t_H N_H + (1 - t_L)N_L} \\ (1 - t_L)\beta_L N_L \dfrac{t_H}{(1 - t_L)N_L + t_H N_H} & (1 - t_L)\beta_L N_L \dfrac{(1 - t_L)}{(1 - t_L)N_L + t_H N_H} \\ + t_L \beta_H N_L \dfrac{(1 - t_H)}{t_L N_L + (1 - t_H)N_H} & + t_L \beta_H N_L \dfrac{t_L}{t_L N_L + (1 - t_H)N_H} \end{pmatrix}$$

The transition matrix V is diagonal with entries $\gamma_H + \alpha_H, \gamma_L + \alpha_L$. For no-treatment, set $\alpha = 0$.

3. Results

This section presents the detailed findings from our two-community model, focusing on (1) time series of infected populations, (2) sensitivity of the basic reproduction number ($\mathcal{R}_0$) to mobility, and (3) final epidemic size. These results provide insights into how economic heterogeneity and mobility between high- and low-income communities influence disease transmission.

3.1. Epidemic Dynamics Without and With Treatment Interventions

While previous studies (e.g., [1, 6]) focus on long-term mobility, our work uniquely examines short-term travel with treatment disparities, revealing non-monotonic patterns on both the basic reproductive number and the final epidemic size. The time series shown in Figure 2 illustrates the dynamics of the high-income and low-income groups in a two-community model without treatment interventions. The differences between the two populations are evident. In the high-income group, the peak of the infected population is lower and occurs slightly earlier compared to the low-income group. For example, the high-income group's I_H peak is more subdued, due to the lower transmission rate assumed for the high-income group ($\beta_H < \beta_L$). Conversely, the low-income group experiences a higher peak in I_L, indicating a larger proportion of individuals becoming infected. The higher I_L peak suggests that the low-income group is more vulnerable to the disease, due to the locally higher transmission rate. By the end of the simulation, a significant proportion of the population in both groups transitions to the recovered state (R_H and R_L). However, the low-income group sees a larger reduction in S_L, implying that a greater fraction of its population was affected by the disease. This disparity highlights the inherent inequalities in disease spread and outcomes between the two groups in the absence of treatment.

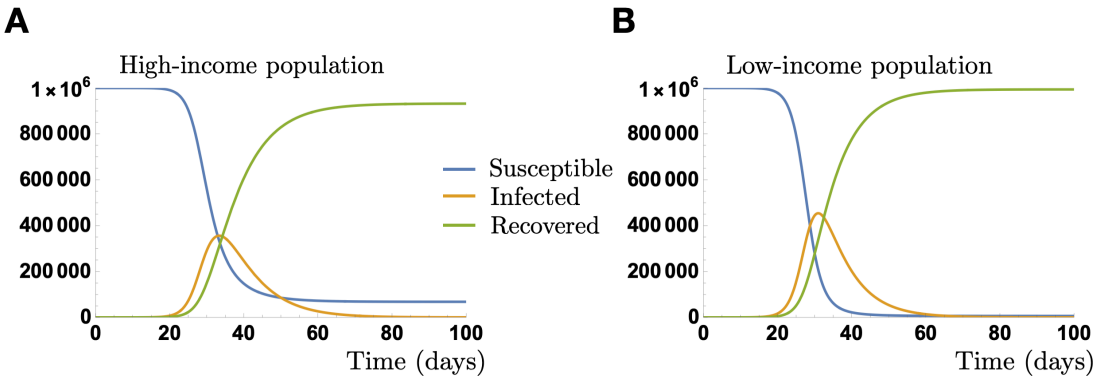

Figure 2: Time series of disease dynamics without treatment. (A) High-income community dynamics (S_H, I_H, R_H), showing a lower and earlier infection peak. (B) Low-income community dynamics (S_L, I_L, R_L), with a higher peak, indicating greater vulnerability. Parameters: $N_H = N_L = 1,000,000$, $\beta_H = 0.2857$, $\beta_L = 3\beta_H = 0.8571$, $\gamma_H = \gamma_L = 1/7 = 0.143$, $t_H = t_L = 0.2$. Simulations run until $t = 100$. Initial conditions: $S_H(0) = N_H$, $I_H(0) = R_H(0) = 0$ and $S_L(0) = N_L - I_L(0)$, $I_L(0) = 10, R_L(0) = 0$; time in days.

Figure 3 shows the impact of incorporating treatment into the model. Here, the introduction of treatment equations dramatically alters the disease dynamics in both groups. The most striking difference is the reduction in the peak number of infected individuals (I_H and I_L) in both populations. For example, in the high-income group, I_H peaks at an even lower level compared to the untreated scenario, and the decline occurs more rapidly. Similarly, the low-income group's I_L peak is also reduced, although it remains higher than I_H. The introduction of treatment also shifts a portion of the population into the treatment compartment (T_H and T_L), which helps mitigate the infection spread. For instance, T_H and T_L curves rise sharply during the initial stages of the outbreak, reflecting active treatment of infected individuals, then decline as treated individuals recover. This treatment reduces the transmission rate, leading to a slower depletion of S_H and S_L. The recovered populations (R_H and R_L) still grow, but at a reduced rate compared to the untreated scenario, as treatment aids in quicker recovery or isolation of infectious individuals. Importantly, the disparity between high- and low-income groups persists even with treatment, though the gap narrows. The high-income group benefits more significantly from treatment due to better access and adherence. For example, the T_H curve rises and falls, stabilizing at a higher proportion compared to T_L, suggesting a more effective intervention for the high-income population. This analysis underscores the importance of equitable treatment distribution to address disparities in disease outcomes.

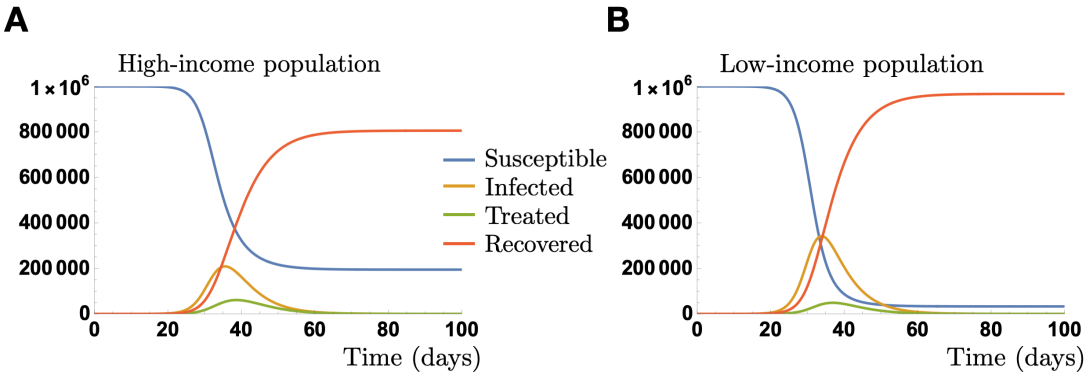

Figure 3: Time series of disease dynamics with treatment. (A) High-income community (S_H, I_H, T_H, R_H), with a reduced infection peak. (B) Low-income community (S_L, I_L, T_L, R_L), with a higher but reduced peak compared to no treatment. Parameters: $N_H = N_L = 1,000,000$, $\beta_H = 0.2857$, $\beta_L = 3\beta_H = 0.8571$, $\gamma_H = \gamma_L = 1/7 = 0.143$, $\alpha_H = 0.10$, $\alpha_L = 0.05$, $\kappa_H = \kappa_L = 0.3$, $t_H = t_L = 0.2$. Simulations run until $t = 100$. Initial conditions: $S_H(0) = N_H$, $I_H(0) = T_H(0) = R_H(0) = 0$ and $S_L(0) = N_L - I_L(0)$, $I_L(0) = 10, T_L(0) = R_L(0) = 0$; time in days.

3.2. Impact of mobility on the basic reproduction number

The basic reproduction number, $\mathcal{R}_0$, represents the expected number of secondary infections generated by a single infected individual. It is a key indicator of epidemic potential for burden. In this framework, it is possible to compute the region-specific and the global basic reproductive numbers. Our results reveal that $\mathcal{R}_0$ is highly sensitive to the travel times (t_H and t_L) and the degree of economic heterogeneity between the two communities, modeled through the ratio of transmission rates ($\beta_L/\beta_H = 3$), and differences in treatment rates ($\alpha_H > \alpha_L$), reflecting disparities in healthcare access and contact rates. We tested sensitivity to varying population size, and infectiousness ratios (see SI Appendix Figure 6).

Figure 4 reveals insights into the dynamics of $\mathcal{R}_0$ under different infection rates, population density, and residence times between patches. Notably, the direction and magnitude of $\mathcal{R}_0$ depend on the relationship between the patch-specific transmission rates (β_H and β_L, see SI Appendix) and the ratio of population sizes of the two patches (N_H/N_L). In Figure 4A, the low-income population is ten times larger than the high-income population, our results show that increasing t_L (more travel by low-income to high-income) decreases $\mathcal{R}_0$, as low-income individuals spend less time

in their high-transmission environment. For example, when $t_H = 0.2$, $\mathcal{R}_0$ decreases as t_L rises. Conversely, $\mathcal{R}_0$ maintain or increases with t_H as more time is spent in the high-risk low-income patch. Interestingly, this non-monotonic behavior occurs at intermediate values of t_H, where $\mathcal{R}_0$ initially decreases but then increases again, suggesting complex interactions between travel patterns and infection dynamics. These findings highlight the importance of carefully managing residence times, particularly in heterogeneous environments with stark differences in transmission risk.

In Figure 4B, where population sizes are equal, the symmetry in population sizes reduces the dominance of either patch, leading to a less pronounced impact of mobility on the $\mathcal{R}_0$. Intermediate residence times ($t_H, t_L \approx 0.3$) result in relatively safer outcomes, with lower overall values of $\mathcal{R}_0$ compared to extreme travel scenarios. Unlike Figure 4A, the effects of t_L and t_H are comparable, with neither parameter overwhelmingly driving the epidemic dynamics. This suggests that mobility policies may be more effective in such balanced systems, as reducing travel (low values of t_H and t_L) between patches can effectively mitigate the epidemic without requiring extreme restrictions.

In Figure 4C, where the high-income population is ten times larger than the low-income population, the $\mathcal{R}_0$ increases or decreases as t_H increases, in contrast to Figure 4A. These non-monotonic dynamics occur for low traveling times scenarios. In this scenario, mobility restrictions would benefit from focusing on controlling t_H to effectively manage the overall epidemic, as t_L exerts relatively little influence on the basic reproduction number.

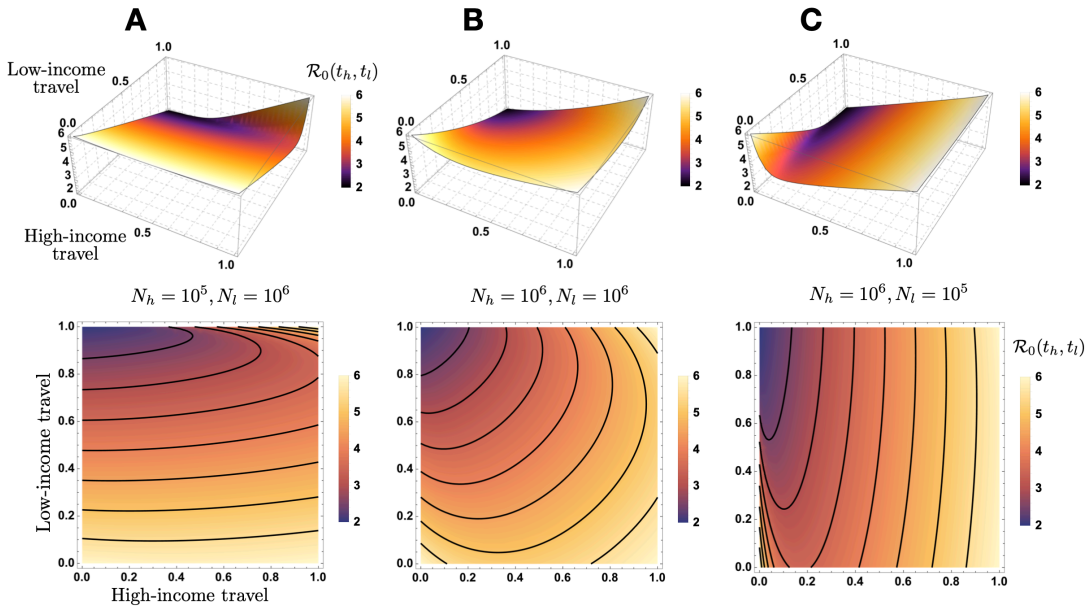

Figure 4: Surface and contours of the basic reproduction number $\mathcal{R}_0$. (A) High-income population = 100,000, low-income = 1,000,000, $\beta_L > \beta_H$, showing decreased $\mathcal{R}_0$ with t_L and non-monotonic behavior at intermediate t_H. (B) Equal populations (1,000,000 each), with lower $\mathcal{R}_0$ at intermediate travel times ($t_H, t_L \approx 0.3$). (C) High-income = 1,000,000, low-income = 100,000, where $\mathcal{R}_0$ rises linearly with t_H. Parameters: $\beta_H = 0.2857$, $\beta_L = 3\beta_H$, $\gamma_H = \gamma_L = 1/7$. This figure illustrates how mobility and population asymmetry drive epidemic potential. Results for the model without treatment interventions.

3.3. Impact of mobility and treatment on the final epidemic size

The final epidemic size is calculated as the total number of recovered individuals at the end of the epidemic ($R(\infty)$ for each community and the combined system). Our results show that, as expected, in scenarios without treatment, the final epidemic size is larger in the low-income community due to higher transmission; while by incorporating treatment both final epidemic sizes are reduced, but disparities persist due to the risk heterogeneity across communities. Interestingly, our results show that traveling from the low-income community, allowing this population to access effective medical resources could significantly reduce the total final epidemic size.

Figure 5A–B illustrates the total final epidemic size ($R_H(\infty) + R_L(\infty)$) for two equally dense populations under different mobility scenarios, shown for both the absence of treatment and the case in which the high-income community has greater access to effective medical resources. In Figure 5A, the total final epidemic size shows symmetry as mobility from both community increases.

Increments on the final epidemic size occur as the low-income population exhibits lower traveling times ($t_L \to 0$) and as the high-income community increases its traveling time ($t_H \to 1$). The intuition behind this result is that this mobility regimes expose susceptible individuals from both communities to the riskier low-income environment. Noteworthy, increasing travel by the low-income group (t_L) could unilaterally decrease the total final epidemic size, as they access the safer high-income environment, while also generating a few cases in the high-income population.

In Figure 5B, with higher health care access in the high-income population ($\alpha_H = 0.1, \alpha_L = 0.05$), the previously observed symmetry on the total final epidemic size is broken. In this scenario, improved health care access in the high-income community mitigates the increase in its local final epidemic size while simultaneously amplifying benefits for the low-income community. Traveling from the low-income community initially increases and then decreases the total final epidemic size. This indicates a mobility threshold where sharing the overall transmission force via population mobility becomes beneficial at the global scale. The inset plot shows the non-monotonic effect of mobility from the low-income community on the total final epidemic size for the low high-income mobility scenario ($t_H = 0.05$), which is indicated by the dashed blue curve in the main figure.

Figure 5C, shows that for the realistic scenario of asymmetrically dense populations ($N_H = 10^5, N_L = 10^6$) and higher mobility from the low-income population ($t_H = 0.1, t_L = 1/3$), increasing treatment rates (α_H, α_L) has contrasting effects. Specifically, increasing α_H has little effect on the total final epidemic size, as the smaller high-income population contributes less to overall burden and experience a reduced infection-risk. In contrast, increasing α_L dramatically reduces the final epidemic size, potentially preventing large outbreaks (final epidemic size ≈ 0) when α_L is high enough. These results suggest that investing in treatment for the larger, higher-risk low-income community, along with managing mobility, could be an effective system-wide control strategy.

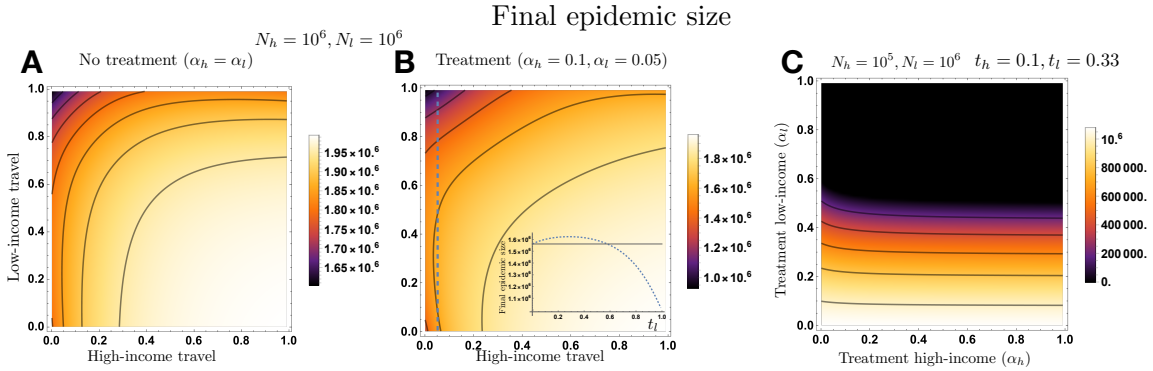

Figure 5: Total final epidemic size under mobility and treatment. (A) Equal population sizes and no treatment: symmetry on the final epidemic size exhibits an overall minimum at high t_L and low t_H. (B) Equal population sizes and heterogeneous treatment ($\alpha_H = 0.1, \alpha_L = 0.05$): broken symmetry of the final epidemic size, non-monotonic in t_L (inset: the total final epidemic size at $t_H = 0.05$ shows non-monotonic dynamics). (C) $N_H = 10^5$, $N_L = 10^6$, fixed $t_H = 0.1$, $t_L = 1/3$: final epidemic size as a function of health care access (α_H, α_L); black region (eradication) is attained when α_L high enough. These results suggest that investing in low-income health care access could more effectively reduce the final epidemic size. Parameters: $\beta_H = 0.2857, \beta_L = 3\beta_H = 0.8571, \gamma_H = \gamma_L = 1/7 \approx 0.143, \kappa_H = \kappa_L = 0.3$.

4. Discussion & Conclusion

In this paper, we formulate a two-community model to study the impact of short-term mobility and healthcare access on epidemic containment in economically heterogeneous populations. We incorporate socioeconomic factors through community-specific transmission rates, population sizes, and treatment access. Population mobility is incorporated using a Lagrangian approach, which tracks individuals' proportion of time spent in each community, serving as a proxy for exposure to community-specific risks. Long-term mobility or migration is not incorporated in this modeling framework.

Our results show that mobility patterns and treatment strategies play critical roles in shaping the local and overall epidemic outcomes. Specifically, our results underscore the vulnerability of often larger and lower-resource populations when access to healthcare is limited, aligning with empirical observations from COVID-19 where low-income communities faced higher burdens due to crowded conditions and limited compliance with restrictions [1, 7, 9]. This highlights the potential of mobility restriction strategies targeting high-transmission areas. A key finding in our analysis is the non-monotonic relationship between the overall final epidemic size and mobility. We

identified conditions under which increasing travel time from the high-risk population can reduce the overall disease burden relative to the total lockdown scenario. Specifically, for equally dense populations without treatment, the total final epidemic size exhibits inverse effects of increasing (decreasing) mobility from the low-income (high-income) population (symmetry along the line $t_h + t_l = 1$), regardless of risk heterogeneity (β_i/β_j). In the presence of heterogeneous health care access, this symmetry breaks, introducing non-monotonicity where low-income travel initially increases and then decreases the final epidemic size. This effect suggests a threshold at which limited low-income travel shares burden without sufficient dilution, while higher travel enables access to better conditions, reducing overall infections. Moreover, in asymmetric scenarios with fixed realistic traveling (low-income traveling more for work), varying treatment rates shows that improving access in the larger low-income community yields greater reductions in total final epidemic size, contrasted with increasing health care access in the high-income community, which shows a minimal impact, emphasizing the efficiency of targeting the riskier, denser group. In general, mobility restrictions (low values of t_H and t_L) could reduce $\mathcal{R}_0$ below the epidemic threshold $\mathcal{R}_0 = 1$. However, the impact of residency times depends on the baseline $\mathcal{R}_0^L$ and $\mathcal{R}_0^H$. This emphasizes the complex trade-off between short-term mobility and health-care access. Population size disparities further add complexity to epidemic control.

In cases where the affected population is significantly larger, it tends to dominate the disease dynamics, making it harder to control the spread into the smaller population. This emphasizes the need for tailored mobility restriction strategies, as uniform policies are less effective in such asymmetric systems, echoing previous work on mobility in heterogeneous populations [2, 6, 15, 16]. In real scenarios, travel proportions may be bounded due to multiple factors. In this study, for theoretical completeness, we allow the full range $\{t_H, t_L\} \in [0, 1]$. Other modeling assumptions include homogeneous mixing and static pathogen traits, which limit applicability to more complex real-world scenarios.

Key insights emerge from this work. First, the disproportionate burden faced by larger low-income populations in the absence of treatment underscores the critical need for healthcare equity. Treatment significantly reduces infection peaks and final epidemic sizes, but its impact varies based on accessibility and allocation. Second, travel dynamics play a pivotal role in minimizing $\mathcal{R}_0$ and final epidemic size. Third, treatment investment is most effective when directed at low-income communities, especially under asymmetry, as it reduces system-wide burden more than equivalent high-income investments. These results provide insights for tailoring interventions taking into account population size and socioeconomic disparities. Finally, this study demonstrates that a combination of treatment, travel optimization, and population-specific interventions can greatly

reduce disease burden and inequity. By accounting for disparities in access and resources, this model emphasizes the importance of targeted strategies in managing infectious disease outbreaks. These findings advocate for mobility and treatment strategies aligned with community-specific needs, rather than restrictions that disproportionately harm vulnerable populations [5, 9].

Future work could expand this framework to include additional factors such as the impact of Non-pharmaceutical Interventions (NPIs) [20], evolving pathogen dynamics, adaptive human behavior in response to infection risk [21, 22, 23, 24, 25, 26, 27], microbiome variations [12], the impact of biosurveillance systems [28], and more complex population structures, further refining these insights and strengthening its relevance for equitable, data-driven public health decision-making.

5. Acknowledgements

We acknowledge the Biocomplexity Institute at the University of Virginia for providing the student with valuable research experience through participation in the Preparing For Global Challenges (P4GC) and Computing for Global Challenges (C4GC) summer programs.

References

1. Espinoza B, Castillo-Chavez C, and Perrings C. Mobility restrictions for the control of epidemics: When do they work? Plos one 2020; 15:e0235731. DOI: 10.1371/journal.pone.0235731
2. Perrings C and Espinoza B. Mobility restrictions and the control of COVID-19. Ecology, Economy and Society-the INSEE Journal 2021; 4:31–43. DOI: 10.37773/ees.v4i1.344
3. Ferguson NM, Laydon D, Nedjati-Gilani G, Imai N, Ainslie K, Baguelin M, et al. Impact of non-pharmaceutical interventions (NPIs) to reduce COVID-19 mortality and healthcare demand. Imperial College London 2020 :1–20. DOI: 10.25561/77482
4. Vearey J, Palmary I, Thomas L, Núñez L, and Drimie S. Urban health in Johannesburg: The importance of place in understanding intra-urban inequalities in a context of migration and HIV. Health & Place 2010; 16:694–702. DOI: 10.1016/j.healthplace.2010.02.007

5. Nana-Sinkam P, Kraschnewski J, Sacco R, Chavez J, Fouad M, Gal T, et al. Health disparities and equity in the era of COVID-19. Journal of Clinical and Translational Science 2021; 5:e99. DOI: 10.1017/cts.2021.23

6. Moreno V, Espinoza B, Barley K, Paredes M, Bichara D, Mubayi A, et al. The role of mobility and health disparities on the transmission dynamics of tuberculosis. Theoretical Biology and Medical Modelling 2017; 14:3. DOI: 10.1186/s12976-017-0049-6

7. Chinazzi M, Davis JT, Ajelli M, Gioannini C, Litvinova M, Merler S, et al. The effect of travel restrictions on the spread of the 2019 novel coronavirus (COVID-19) outbreak. Science 2020; 368:395–400. DOI: 10.1126/science.aba9757

8. Ying YH, Lee WL, Chi YC, Chen MJ, and Chang K. Demographics, Socioeconomic Context, and the Spread of Infectious Disease: The Case of COVID-19. International Journal of Environmental Research and Public Health 2022; 19:2206. DOI: 10.3390/ijerph19042206. Available from: https://www.mdpi.com/1660-4601/19/4/2206

9. Patel JA, Nielsen FB, Badiani AA, Assi S, Unadkat VA, Patel B, et al. Poverty, inequality, and COVID-19: The forgotten vulnerable. Public Health 2020; 183:110–1. DOI: 10.1016/j.puhe.2020.05.006

10. Flaskerud JH and DeLilly CR. Social determinants of health status. Issues in mental health nursing 2012; 33:494–7. DOI: 10.3109/01612840.2012.662581

11. Amato KR, Arrieta MC, Azad MB, Bailey MT, Broussard JL, Bruggeling CE, et al. The human gut microbiome and health inequities. Proceedings of the National Academy of Sciences 2021; 118:e2017947118. DOI: 10.1073/pnas.2017947118

12. Kwak S, Usyk M, Beggs D, Choi H, Ahdoot D, Wu F, et al. Sociobiome-Individual and neighborhood socioeconomic status influence the gut microbiome in a multi-ethnic population in the US. npj Biofilms and Microbiomes 2024; 10:19. DOI: 10.1038/s41522-024-00491-y

13. Sarkar A, Harty S, Moeller AH, Klein SL, Erdman SE, Friston KJ, et al. The gut microbiome as a biomarker of differential susceptibility to SARS-CoV-2. Trends in Molecular Medicine 2021; 27:1115–34. DOI: 10.1016/j.molmed.2021.09.009

14. Wells CR, Sah P, Moghadas SM, Pandey A, Shoukat A, Wang Y, et al. Impact of international travel and border control measures on the global spread of the novel 2019 coronavirus outbreak. Proceedings of the National Academy of Sciences 2020; 117:7504–9. DOI: 10.1073/pnas.2002616117

15. Moreno VM, Espinoza B, Bichara D, Holechek SA, and Castillo-Chavez C. Role of short-term dispersal on the dynamics of Zika virus in an extreme idealized environment. Infectious Disease Modelling 2017; 2:21–34. DOI: 10.1016/j.idm.2016.12.002

16. Espinoza B, Moreno V, Bichara D, and Castillo-Chavez C. Assessing the efficiency of movement restriction as a control strategy of Ebola. *Mathematical and Statistical Modeling for Emerging and Re-emerging Infectious Diseases*. Springer, 2016 :123–45. DOI: 10.1007/978-3-319-40413-4_9

17. Diekmann O, Heesterbeek JAP, and Metz JAJ. On the definition and the computation of the basic reproduction ratio R_0 in models for infectious diseases in heterogeneous populations. Journal of Mathematical Biology 1990; 28:365–82. DOI: 10.1007/BF00178324

18. Heesterbeek JAP. A brief history of R_0 and a recipe for its calculation. Acta Biotheoretica 2002; 50:189–204. DOI: 10.1023/A:1016599411804

19. Van den Driessche P and Watmough J. Reproduction numbers and sub-threshold endemic equilibria for compartmental models of disease transmission. Mathematical Biosciences 2002; 180:29–48. DOI: 10.1016/S0025-5564(02)00108-6

20. Dixit AK, Espinoza B, Qiu Z, Vullikanti A, and Marathe MV. Airborne disease transmission during indoor gatherings over multiple time scales: Modeling framework and policy implications. Proceedings of the National Academy of Sciences 2023; 120:e2216948120. DOI: 10.1073/pnas.2216948120

21. Espinoza B, Marathe M, Swarup S, and Thakur M. Asymptomatic individuals can increase the final epidemic size under adaptive human behavior. Scientific Reports 2021; 11:19744. DOI: 10.1038/s41598-021-98999-2

22. Espinoza B, Swarup S, Barrett CL, and Marathe M. Heterogeneous adaptive behavioral responses may increase epidemic burden. Scientific Reports 2022; 12:11276. DOI: 10.1038/s41598-022-15444-8

23. Espinoza B, Saad-Roy CM, Grenfell BT, Levin SA, and Marathe M. Adaptive human behaviour modulates the impact of immune life history and vaccination on long-term epidemic dynamics. Proceedings of the Royal Society B: Biological Sciences 2024; 291:20241772. DOI: 10.1098/rspb.2024.1772

24. Espinoza B, Chen J, Orr M, Saad-Roy CM, Levin SA, and Marathe M. The impact of risk compensation adaptive behavior on the final epidemic size. Mathematical Biosciences 2025; 380:109370. DOI: 10.1016/j.mbs.2024.109370

25. Chen J, Espinoza B, Chou J, Gumel AB, Levin SA, and Marathe M. A simple model of coupled individual behavior and its impact on epidemic dynamics. Mathematical Biosciences 2025; 380:109345. DOI: 10.1016/j.mbs.2024.109345

26. Nguyen MM, Freedman AS, Cheung MA, Saad-Roy CM, Espinoza B, Grenfell BT, et al. The complex interplay between risk tolerance and the spread of infectious diseases. Journal of the Royal Society Interface 2025; 22:20240486. DOI: 10.1098/rsif.2024.0486

27. Mahmud MS, Eshun S, Espinoza B, and Kadelka C. Adaptive human behavior and delays in information availability autonomously modulate epidemic waves. PNAS Nexus 2025; 4:pgaf145. DOI: 10.1093/pnasnexus/pgaf145

28. Espinoza B, Adiga A, Venkatramanan S, Warren AS, Chen J, Lewis BL, et al. Coupled models of genomic surveillance and evolving pandemics with applications for timely public health interventions. Proceedings of the National Academy of Sciences 2023; 120:e2305227120. DOI: 10.1073/pnas.2305227120

A. Appendix

A.1. Two-community epidemic model - no treatment

For the no-treatment model, a special case of the treatment model with $\alpha_H = \alpha_L = 0$, we formulated a system of differential equations to model disease dynamics in two economically heterogeneous communities. We employed a Lagrangian approach, using a residency time matrix to track mobility. The model incorporates the proportion of time individuals spend in each community (t_H, t_L) as a proxy for disease vulnerability. The flow diagram in Figure 1A shows the epidemiological states—susceptible (S), infected (I), and recovered (R)—and model parameters.

$$
\begin{aligned}
\dot{S_H} &= -(1-t_H)\beta_H S_H \frac{(1-t_H)I_H + t_L I_L}{(1-t_H)N_H + t_L N_L} - t_H \beta_L S_H \frac{t_H I_H + (1-t_L)I_L}{t_H N_H + (1-t_L)N_L} \\
\dot{I_H} &= (1-t_H)\beta_H S_H \frac{(1-t_H)I_H + t_L I_L}{(1-t_H)N_H + t_L N_L} + t_H \beta_L S_H \frac{t_H I_H + (1-t_L)I_L}{t_H N_H + (1-t_L)N_L} - \gamma_H I_H \\
\dot{R_H} &= \gamma_H I_H \\
\dot{S_L} &= -(1-t_L)\beta_L S_L \frac{(1-t_L)I_L + t_H I_H}{(1-t_L)N_L + t_H N_H} - t_L \beta_H S_L \frac{t_L I_L + (1-t_H)I_H}{t_L N_L + (1-t_H)N_H} \\
\dot{I_L} &= (1-t_L)\beta_L S_L \frac{(1-t_L)I_L + t_H I_H}{(1-t_L)N_L + t_H N_H} + t_L \beta_H S_L \frac{t_L I_L + (1-t_H)I_H}{t_L N_L + (1-t_H)N_H} - \gamma_L I_L \\
\dot{R_L} &= \gamma_L I_L
\end{aligned}
\tag{2}
$$

Parameters are as defined in Section 2.1, excluding treatment terms $(\alpha_H, \alpha_L, \kappa_H, \kappa_L)$.

A.2. The basic reproductive number via the Next-Generation Matrix

We compute the model's (2) basic reproductive number $\mathcal{R}_0$ using the next-generation matrix method [17, 18, 19]. The transmission matrix F is derived from the infection terms at the disease-free equilibrium (DFE: $S_H = N_H, S_L = N_L, I_H = I_L = R_H = R_L = 0$). The full expressions for new infections are:

$$F = \begin{pmatrix} (1-t_H)\beta_H N_H \dfrac{(1-t_H)}{(1-t_H)N_H + t_L N_L} & (1-t_H)\beta_H N_H \dfrac{t_L}{(1-t_H)N_H + t_L N_L} \\ + t_H \beta_L N_H \dfrac{t_H}{t_H N_H + (1-t_L)N_L} & + t_H \beta_L N_H \dfrac{1-t_L}{t_H N_H + (1-t_L)N_L} \\ (1-t_L)\beta_L N_L \dfrac{t_H}{(1-t_L)N_L + t_H N_H} & (1-t_L)\beta_L N_L \dfrac{(1-t_L)}{(1-t_L)N_L + t_H N_H} \\ + t_L \beta_H N_L \dfrac{(1-t_H)}{t_L N_L + (1-t_H)N_H} & + t_L \beta_H N_L \dfrac{t_L}{t_L N_L + (1-t_H)N_H} \end{pmatrix}$$

The transition matrix V is diagonal with entries $V_{11} = \gamma_H + \alpha_H, V_{22} = \gamma_L + \alpha_L$. We decided to keep the treatment rates (α) in the analysis for completeness, noting that for the no-treatment scenario, we simply set $\alpha = 0$. $\mathcal{R}_0$ is the largest eigenvalue of FV^{-1}.

For uncoupled cases ($t_H = t_L = 0$), the matrix diagonalizes, recovering $\mathcal{R}_0^H = \beta_H/(\gamma_H + \alpha_H)$ and $\mathcal{R}_0^L = \beta_L/(\gamma_L + \alpha_L)$, consistent with single-patch SITR models.

A.3. The impact of infectiousness ratio on basic reproductive number

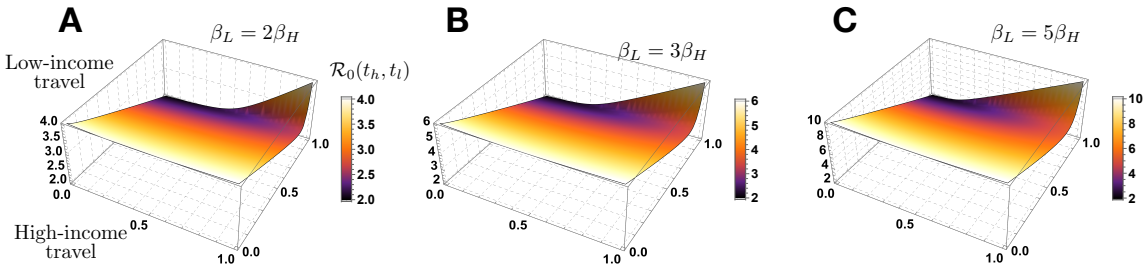

Figure 6: Basic reproductive number as function of traveling times for varying infectiousness ratios. (A) Low infectiousness disparities scenario $\beta_L = 2\beta_H$. (B) Intermediate infectiousness disparities scenario $\beta_L = 3\beta_H$. This is the baseline scenario. (C) High infectiousness disparities scenario $\beta_L = 5\beta_H$. These results show that infectiousness disparities quantitatively impact the global basic reproductive number while qualitatively keeping the impact of traveling times. Parameters: $\gamma_H = \gamma_L = 1/7 \approx 0.143, \kappa_H = \kappa_L = 0.3$.